Photophysical Properties of Borondipyrromethene Analogues in Solution

Wenwu Qin, Mukulesh Baruah, Mark Van der Auweraer, Frans C. De Schryver, and Noël Boens*

Department of Chemistry, Katholieke Universiteit Leuven, Celestijnenlaan 200F, 3001 Heverlee (Leuven), Belgium

Received: May 19, 2005; In Final Form: June 28, 2005

The photophysical properties of seven new 8-(*p*-substituted)phenyl analogues of 4,4-difluoro-3,5-dimethyl-8-(aryl)-4-bora-3a,4a-diaza-*s*-indacene (derivatives of the well-known fluorophore BODIPY) in several solvents have been studied by means of absorption and steady-state and time-resolved fluorimetry. For each compound, the fluorescence quantum yield and lifetime are lower in solvents with higher polarity owing to an increase in the rate of nonradiative deactivation. Increasing the electron withdrawing strength of the *p*-substituent on the phenyl group in position 8 also leads to lower fluorescence quantum yields and lifetimes. When the *p*-substituent on the phenyl group in position 8 is a tertiary amine [8-(4-piperidinophenyl), 8-(4-*N*,*N*-dimethylaminophenyl), and 8-(4-morpholinophenyl)], the low quantum yields of these compounds in more polar solvents can be rationalized by the inversion of the energy levels of an apolar, highly fluorescent and a polar, nonfluorescent excited state, where charge transfer from the tertiary amine to the BODIPY unit occurs. These amine analogues can be protonated at low pH in aqueous solution. Fluorescence titrations yielded pK_a values of their conjugate ammonium salts which are in agreement with the electron donating tendency of the amine group: piperidino (4.15) > dimethylamino (2.37) > morpholino (1.47), with the pK_a values in parentheses. The rate constant of radiative deactivation (k_f) is the same for all compounds in all solvents studied ($k_f = 1.4 \times 10^8$ s^{-1}).

Introduction

The design and development of fluorescent chemosensors for the detection of analytically important species is still an expanding area of research.[1] Due to their favorable photophysical and optoelectronic properties, 4,4-difluoro-4-bora-3a,4a-diaza-*s*-indacene[2] (difluoroborondipyrromethene, BDP, or BODIPY[3]) derivatives have become favorite fluorophores in new fluorescent probes that have applications in many different areas.[4] For example, BODIPY dyes can offer improved spectral characteristics compared to other conventional dyes when used in automated DNA sequencing.[5] The excellent qualities of BODIPY comprise high fluorescence quantum yields and narrow emission bandwidths with high peak intensities, elevated photostability, relatively high absorption coefficients, and the extra feature of excitation/emission wavelengths in the visible region. Moreover, their building block synthesis allows one to develop many different BODIPY analogues with different receptor groups and with emission ranges from 500 to over 700 nm. The photophysical properties of several BODIPY derivatives in liquid solution have been studied by means of absorption and fluorescence techniques.[6−8]

In the present work, we synthesized novel fluorescent compounds with BODIPY as the common fluorophore but with different *para*-substituents (R) on the benzene ring at position 8 (Scheme 1). The first BODIPY series includes compounds **1**, **2**, **3**, and **4** (Scheme 1), with the *p*-substituent (R) ranging from electron donating (methoxy) to electron withdrawing (cyano). The second series covers BODIPY analogues **5**, **6**, and **7** in which the *p*-substituent (R) is a tertiary amine. To investigate the photophysical properties of the new BODIPY compounds, we recorded their steady-state absorption and fluorescence excitation and emission spectra and collected their time-resolved fluorescence profiles in several solvents. From these experiments, we could determine the position of the spectra (λ_{abs}, λ_{ex}, and λ_{em}), the full width at half-maximum of the absorption band (fwhm$_{abs}$), the fluorescence quantum yields (ϕ_f), the rate constants of radiative (k_f) and nonradiative (k_{nr}) deactivation, Stokes shifts ($\Delta\bar{\nu}$), fluorescence lifetimes (τ), and molar absorption coefficients (ϵ) of the compounds. Furthermore, the reversible protonation/deprotonation of **5**, **6**, and **7** in aqueous solution was also studied.

Experimental Section

Syntheses. *General Methods.* ^{1}H and ^{13}C NMR spectra were recorded at room temperature on a Bruker Avance 300 instrument operating at a frequency of 300 MHz for ^{1}H and 75 MHz for ^{13}C. ^{1}H NMR spectra were referenced to tetramethylsilane (0.00 ppm) as an internal standard. Chemical shift multiplicities are reported as s = singlet, d = doublet, t = triplet, q = quartet, and m = multiplet. ^{13}C spectra were referenced to the $CDCl_3$ (77.67 ppm) signal. Mass spectra were recorded on a Hewlett-Packard 5989A mass spectrometer (E.I. mode and C.I. mode). High resolution mass data were obtained with a KRATOS MS50TC instrument. Melting points were taken on a Reichert Thermovar and are uncorrected.

*5-Phenyl-1,9-dimethyldipyrromethene (**9b**).* This condensation was carried out according to a published procedure[9] (Scheme 1). In a 250 mL round-bottomed flask, benzaldehyde (**8b**) (159 mg, 1.5 mmol) and 2-methylpyrrole (260 mg, 3.21 mmol) were dissolved in 100 mL of dry dichloromethane under an argon atmosphere. One drop of trifluoroacetic acid (TFA) was added

* To whom correspondence should be addressed. E-mail: Noel.Boens@chem.kuleuven.be. Fax: +32-16-327990.

10.1021/jp052626n CCC: $30.25
Published on Web 08/04/2005

SCHEME 1: Synthesis of the BODIPY Derivatives

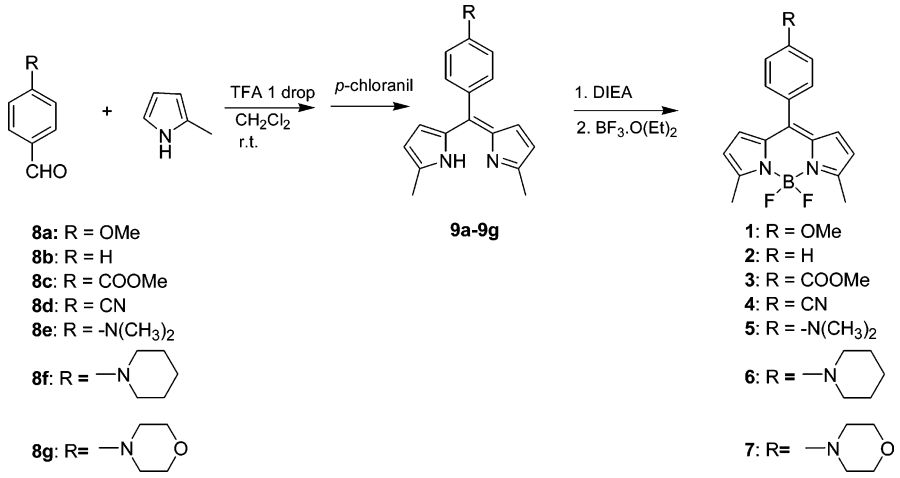

to the stirred mixture. Stirring was continued overnight at room temperature. After the disappearance of benzaldehyde [monitored by thin-layer chromatography (TLC)], a solution of *p*-chloranil (217.5 mg, 1.5 mmol) in dichloromethane (25 mL) was added. The mixture was further stirred for 0.5 h and then quenched with water. The organic layer was separated, and the water layer was further extracted with dichloromethane. The combined organic layers were dried over $MgSO_4$ and concentrated and purified through column chromatography over neutral alumina (hexane/ethyl acetate, 7/3, v/v) to obtain a reddish brown powder in 39% yield (145 mg). ^{1}H NMR ($CDCl_3$): δ 7.44 (m, 5H); 6.55 (d, 2H, J = 4.0 Hz); 6.24 (d, 2H, J = 4.0 Hz); 2.53 (s, 6H). ^{13}C NMR ($CDCl_3$): δ 158.0, 139.0, 130.8, 130.5, 130.3, 128.6, 119.8, 30.1, 15.3. MS (CI) *m*/*z* (%): 249 (MH^+, 100).

Dipyrromethene analogues **9a**, **9c**, **9d**, **9e**, **9f**, and **9g** were similarly prepared starting from 4-methoxybenzaldehyde (**8a**), methyl 4-formylbenzoate (**8c**), 4-formylbenzonitrile (**8d**), 4-dimethylaminobenzaldehyde (**8e**), 4-piperidin-1-yl-benzaldehyde (**8f**), and 4-morpholin-4-yl-benzaldehyde (**8g**), respectively.

*5-(p-Methoxyphenyl)-1,9-dimethyldipyrromethene (**9a**).* Yield 32%. ^{1}H NMR ($CDCl_3$): δ 7.7 (s, NH); 7.40 (d, 2H, J = 8.7 Hz); 6.94 (d, 2H, J = 8.7 Hz); 6.50 (d, 2H, J = 4.3 Hz); 6.16 (d, 2H, J = 4.4 Hz); 3.91 (s, 3H); 2.45 (s, 6H). MS (CI) *m*/*z* (%): 279 (MH^+, 100).

*5-(4-Carbomethoxyphenyl)-1,9-dimethyldipyrromethene (**9c**).* Yield 24%. ^{1}H NMR ($CDCl_3$): δ 8.09 (d, 2H, J = 8.0 Hz); 7.53 (d, 2H, J = 8.0 Hz); 6.39 (d, 2H, J = 3.6 Hz); 6.16 (d, 2H, J = 4.3 Hz); 3.97 (s, 3H); 2.46 (s, 6H). MS (CI) *m*/*z* (%): 307 (MH^+, 100).

*5-(4-Cyanophenyl)-1,9-dimethyldipyrromethene (**9d**).* Yield 58%. ^{1}H NMR ($CDCl_3$): δ 7.63 (d, 2H, J = 7.7 Hz); 7.41 (d, 2H, J = 7.9 Hz); 6.58 (d, 2H, J = 3.8 Hz); 6.21 (d, 2H, J = 3.3 Hz); 2.46 (s, 6H). MS (CI) *m*/*z* (%): 274 (MH^+, 100).

*5-(4-N,N-Dimethylphenyl)-1,9-dimethyldipyrromethene (**9e**).* Yield 54%. ^{1}H NMR ($CDCl_3$): δ 7.38 (d, 2H, J = 8.0 Hz); 6.73 (d, 2H, J = 8.8 Hz); 6.60 (d, 2H, J = 3.6 Hz); 6.17 (d, 2H, J = 3.6 Hz); 3.04 (s, 6H); 2.45 (s, 6H). MS (CI) *m*/*z* (%): 292 (MH^+, 100).

*5-(4-Pipiridinophenyl)-1,9-dimethyldipyrromethene (**9f**).* Yield 64%. ^{1}H NMR ($CDCl_3$): δ 7.31 (d, 2H, J = 8.1 Hz); 6.84 (d, 2H, J = 7.9 Hz); 6.58 (d, 2H, J = 3.7 Hz); 6.16 (d, 2H, J = 4.1 Hz); 3.19 (m, 4H); 2.45 (s, 6H); 1.72 (m, 4H); 1.59 (m, 2H). MS (CI) *m*/*z* (%): 332 (MH^+, 100).

*5-(4-Morpholinophenyl)-1,9-dimethyldipyrromethene (**9g**).* Yield 71%. ^{1}H NMR ($CDCl_3$): δ 7.39 (d, 2H, J = 8.8 Hz); 6.92 (d, 2H, J = 8.0 Hz); 6.54 (d, 2H, J = 3.6 Hz); 6.16 (d, 2H, J = 4.4 Hz); 3.89 (t, 4H, J = 4.7 Hz); 3.25 (t, 4H, J = 4.7 Hz); 2.45 (s, 6H). MS (CI) *m*/*z* (%): 334 (MH^+, 100).

*4,4-Difluoro-3,5-dimethyl-8-phenyl-4-bora-3a,4a-diaza-s-indacene (**2**).* A 0.5 mmol (124 mg) portion of dipyrromethene (**9b**) was dissolved in 70 mL of dichloromethane. *N*,*N*-Diisopropylethylamine (DIEA, 2.5 mL, 16 mmol) was added, and the mixture was stirred at room temperature for 20 min under argon. BF_3·OEt_2 (2.5 mL, 20 mmol) was added dropwise, and stirring was continued for 1 h. The reaction mixture was washed with water and 2 N NaOH. The aqueous solution was extracted with dichloromethane, dried over $MgSO_4$, filtered, and evaporated. The crude material was purified via silica gel chromatography (ethyl acetate/hexane, 3/7, v/v). Recrystallization from hexane gives green crystals in 62% yield (92 mg). mp 107 °C. ^{1}H NMR ($CDCl_3$): δ 7.50 (m, 5H); 6.72 (d, 2H, J = 3.6 Hz); 6.29 (d, 2H, J = 4.4 Hz); 2.67 (s, 6H). ^{13}C NMR ($CDCl_3$): δ 155.2, 140.4, 138.8, 137.9, 131.2, 129.5, 128.9, 127.9, 117.9, 14.7. LRMS (EI, 70 eV) *m*/*z* (%): 297 (M^+, 21), 296 (M^+, 100), 295 (M^+, 33). HRMS (EI^+): calcd for $C_{17}H_{15}BF_2N_2$ (M^+), 296.12964; found, 296.12875.

BODIPY derivatives **1**, **3**, **4**, **5**, **6**, and **7** were prepared using the same procedure, starting from dipyrromethenes **9a**, **9c**, **9d**, **9e**, **9f**, and **9g**, respectively.

*4,4-Difluoro-3,5-dimethyl-8-(4-methoxyphenyl)-4-bora-3a,4a-diaza-s-indacene (**1**).* Recrystallization from hexane/$CHCl_3$ yields red crystals in 82% yield. mp 191 °C. ^{1}H NMR ($CDCl_3$): δ 7.45 (d, 2H, J = 8.7 Hz); 7.0 (d, 2H, J = 8.7 Hz); 6.75 (d, 2H, J = 3.6 Hz); 6.27 (d, 2H, J = 4.4 Hz); 3.90 (s, 3H); 2.66 (s, 6H). ^{13}C NMR ($CDCl_3$): δ 156.0, 152.2, 144.2, 134.7, 132.7, 130.3, 122, 3118.9, 111.7, 52.7, 15.2. LRMS (EI, 70 eV) *m*/*z* (%): 327 (M^+, 23), 326 (M^+, 100), 325 (M^+, 50), 307 (14), 306 (48), 305 (24). HRMS (EI^+): calcd for $C_{18}H_{17}BF_2N_2O$ (M^+), 326.14020; found, 326.13975.

*4,4-Difluoro-3,5-dimethyl-8-(4-carbomethoxyphenyl)-4-bora-3a,4a-diaza-s-indacene (**3**).* Recrystallization from hexane/$CHCl_3$ yields green crystals in 67% yield. mp 205 °C. ^{1}H NMR ($CDCl_3$): δ 8.14 (d, 2H, J = 8.1 Hz); 7.57 (d, 2H, J = 8.0 Hz); 6.66 (d, 2H, J = 3.6 Hz); 6.28 (d, 2H, J = 3.6 Hz); 3.99 (s, 3H); 2.67 (s, 6H). ^{13}C NMR ($CDCl_3$): δ 166.7, 158.6, 141.3, 138.8, 134.6, 130.7, 129.7, 120.1, 52.8, 30.0, 15.3. LRMS (EI, 70 eV) *m*/*z* (%): 353 (M^+, 50), 354 (M^+, 100), 355 (M^+, 15), 333(42), 334(61). HRMS (EI^+): calcd for $C_{19}H_{17}BF_2N_2O_2$ (M^+), 354.13511; found, 354.13522.

*4,4-Difluoro-3,5-dimethyl-8-(4-cyanophenyl)-4-bora-3a,4a-diaza-s-indacene (**4**).* Recrystallization from hexane/$CHCl_3$

yields green crystals in 52% yield. mp 193 °C. ^{1}H NMR ($CDCl_3$): δ 7.79 (d, 2H, $J = 8.0$ Hz); 7.6 (d, 2H, $J = 8.0$ Hz); 6.61 (d, 2H, $J = 4.4$ Hz); 6.30 (d, 2H, $J = 3.7$ Hz); 2.67 (s, 6H). ^{13}C NMR ($CDCl_3$): δ 159.3, 139.0, 134.4, 132.4, 131.2, 130.3, 120.5, 114.2, 118.4, 15.3. LRMS (EI, 70 eV) *m*/*z* (%): 322 (M^+, 30), 321 (M^+, 100), 320 (M^+, 64), 319 (M^+, 22), 302 (32), 301 (82), 299 (25). HRMS (EI^+): calcd for $C_{18}H_{14}BF_2N_3$ (M^+), 321.12488; found, 321.12519.

*4,4-Difluoro-3,5-dimethyl-8-(4-N,N-dimethylaminophenyl)-4-bora-3a,4a-diaza-s-indacene (**5**).* Recrystallization from hexane/$CHCl_3$ yields orange red crystals in 86% yield. mp 279 °C. ^{1}H NMR ($CDCl_3$): δ 7.44 (d, 2H, $J = 8.8$ Hz); 6.84 (d, 2H, $J = 4.0$ Hz); 6.76 (d, 2H, $J = 8.5$ Hz); 6.26 (d, 2H, $J = 4.0$ Hz); 3.08 (s, 6H); 2.65 (s, 6H). ^{13}C NMR ($CDCl_3$): δ 144.2, 156.0, 152.2, 134.7, 132.7, 130.3, 122.3, 118.9, 111.7, 40.5, 15.2. LRMS (EI, 70 eV) *m*/*z* (%): 340 (M^+, 24), 339 (M^+, 100), 338 (M^+, 45), 319 (41), 318 (18). HRMS (EI^+): calcd for $C_{19}H_{20}BF_2N_3$ (M^+), 339.17183; found, 339.17184.

*4,4-Difluoro-3,5-dimethyl-8-(4-pipiridinophenyl)-4-bora-3a,4a-diaza-s-indacene (**6**).* Recrystallization from hexane/$CHCl_3$ yields red crystals in 72% yield. mp 280 °C. ^{1}H NMR ($CDCl_3$): δ 7.41 (d, 2H, $J = 8.8$ Hz); 6.95 (d, 2H, $J = 8.8$ Hz); 6.82 (d, 2H, $J = 4.4$ Hz); 6.26 (d, 2H, $J = 3.6$ Hz); 3.32 (t, 4H, $J = 5.5$ Hz); 2.65 (s, 6H); 1.66 (m, 6H). ^{13}C NMR ($CDCl_3$): δ 156.3, 153.4, 144.1, 134.7, 132.6, 130.4, 124.1, 119.1, 114.7, 49.6, 25.9, 24.7, 15.2. LRMS (EI, 70 eV) *m*/*z* (%): 380 (M^+, 21), 379 (M^+, 100), 378 (M^+, 62), 359 (17), 302 (11). HRMS (EI^+): calcd for $C_{22}H_{24}BF_2N_3$ (M^+), 379.20313; found, 379.20291.

*4,4-Difluoro-3,5-dimethyl-8-(4-morpholinophenyl)-4-bora-3a,4a-diaza-s-indacene (**7**).* Recrystallization from hexane/$CHCl_3$ yields orange crystals in 93% yield. mp 264 °C. ^{1}H NMR ($CDCl_3$): δ 7.4 (d, 2H, $J = 8.7$ Hz); 6.9 (d, 2H, $J = 8.8$ Hz); 6.7 (d, 2H, $J = 4.4$ Hz); 6.2 (d, 2H, $J = 3.7$ Hz); 3.8 (t, 4H, $J = 4.7$ Hz); 3.2 (t, 4H, $J = 4.7$ Hz); 2.6 (s, 6H). ^{13}C NMR ($CDCl_3$): δ 156.8, 152.9, 149.1, 134.8, 132.4, 130.5, 125.4, 119.3, 114.5, 67.1, 48.5, 15.2. LRMS (EI, 70 eV) *m*/*z* (%): 382 (M^+, 26), 381 (M^+, 100), 379 (M^+, 1), 361 (14), 323 (16), 322 (11), 303 (24), 302 (21). HRMS (EI^+): calcd for $C_{21}H_{22}BF_2N_3O$ (M^+), 381.18240; found, 381.18158.

Materials. All solvents (Aldrich, Sigma-Aldrich, Acros Organics, or Riedel-Dehaën) for the spectroscopic measurements were of spectroscopic grade and were used without further purification. The chemicals used for the synthesis were of the best grade available, supplied by Acros Organics or Aldrich, and used as received. Dichloromethane (p.a.) was dried over molecular sieves. Boron trifluoride etherate, ~48% BF_3, was from Acros Organics.

Steady-State Spectroscopy. The absorption measurements were performed on a Perkin-Elmer Lambda 40 UV−vis spectrophotometer. Corrected steady-state excitation and emission spectra were recorded on a SPEX Fluorolog instrument. For the determination of the relative fluorescence quantum yields (ϕ_f), only dilute solutions with an absorbance below 0.1 at the excitation wavelength (λ_{ex}) were used. Rhodamine 6G in H_2O ($\lambda_{ex} = 488$ nm, $\phi_f = 0.76$) was used as a fluorescence standard.[10] For the samples that were not degassed, the ϕ_f values reported in this work are the average values of multiple (generally four) fully independent measurements. For the determination of ϕ_f of samples that were degassed by consecutive freeze−pump−thaw cycles, only one ϕ_f measurement was done. In all cases, correction for the refractive index was applied.

Time-Resolved Spectroscopy. Fluorescence decay traces of the BODIPY compounds were recorded by the single-photon timing method.[11] Details of the instrumentation[12] and experimental procedures[13] used have been described elsewhere. Briefly, the second harmonic of a Ti:sapphire laser (Tsunami, Spectra Physics) was used to excite the samples at 488 nm with a repetition rate of 8.18 MHz. The detection system consisted of a subtractive double monochromator (9030DS, Sciencetech) and a microchannel plate photomultiplier (R38090U, Hamamatsu). A time-correlated single-photon timing PC module (SPC 630, Picoquant) was used to obtain the fluorescence decay histograms in 4096 channels, with a time increment per channel of 3.0 ps. In combination with the stepper motor controller device SM (STP 240, Picoquant GmbH), which sets the monochromator wavelength, the SPC card enabled us to record fluorescence decays on the picosecond time scale. Fluorescence decays at several emission wavelengths were recorded using 10 × 10 mm cuvettes. The absorbance at the excitation wavelength was always below 0.1. All lifetime measurements were performed on samples that were degassed by consecutive freeze−pump−thaw cycles. Histograms of the instrument response functions (using LUDOX scatterer) and sample decays were recorded until they typically reached 10^4 counts in the peak channel. The total width at half-maximum of the instrument response function was ~60 ps.

The fitting parameters were determined by minimizing the global *reduced* chi-square (χ_g^2):

$$\chi_g^2 = \sum_l^q \sum_i w_{li}(y_{li}^o - y_{li}^c)/\nu \qquad (1)$$

where the index l sums over q experiments and the index i sums over the appropriate channel limits for each individual experiment. y_{li}^o and y_{li}^c denote respectively the observed and calculated (fitted) values corresponding to the ith channel of the lth experiment, and w_{li} is the corresponding statistical weight. ν represents the number of degrees of freedom for the entire multidimensional fluorescence decay surface.

The statistical criteria to judge the quality of the fit included both graphical and numerical tests. The graphical methods covered plots of surfaces ("carpets") of the autocorrelation function values versus channel number versus experiment number and of the weighted residuals versus channel number versus experiment number. The additional statistical criteria to judge the quality of the fit are described elsewhere.[14]

When the fluorescence decays were monoexponential, the rate constants of radiative (k_f) and nonradiative (k_{nr}) deactivation were calculated from the measured fluorescence quantum yield (ϕ_f) and fluorescence lifetime (τ) according to eqs 2 and 3:

$$k_f = \phi_f/\tau \qquad (2)$$

$$k_{nr} = (1 - \phi_f)/\tau \qquad (3)$$

All measurements were done at 20 °C.

Determination of K_a from Fluorimetric Titration. To determine the ground-state acidity constants (K_a) of (the ammonium salts of) **5**, **6**, and **7**, the fluorescent indicators were dissolved in 1.0 M HCl solution in Milli-Q water. Then, 0.1 and 0.01 M solutions of HCl and NaOH were used to adjust the pH of the solutions. All measurements were performed in aqueous nonbuffered solutions at 20 °C, using 10 mm optical path quartz cells.

The expression of the steady-state fluorescence signal (F) as a function of the ion concentration has been derived by Kowalczyk et al. for the case of a 1:1 complex between a fluorescent indicator and an analyte (here H^+).[15] The expression

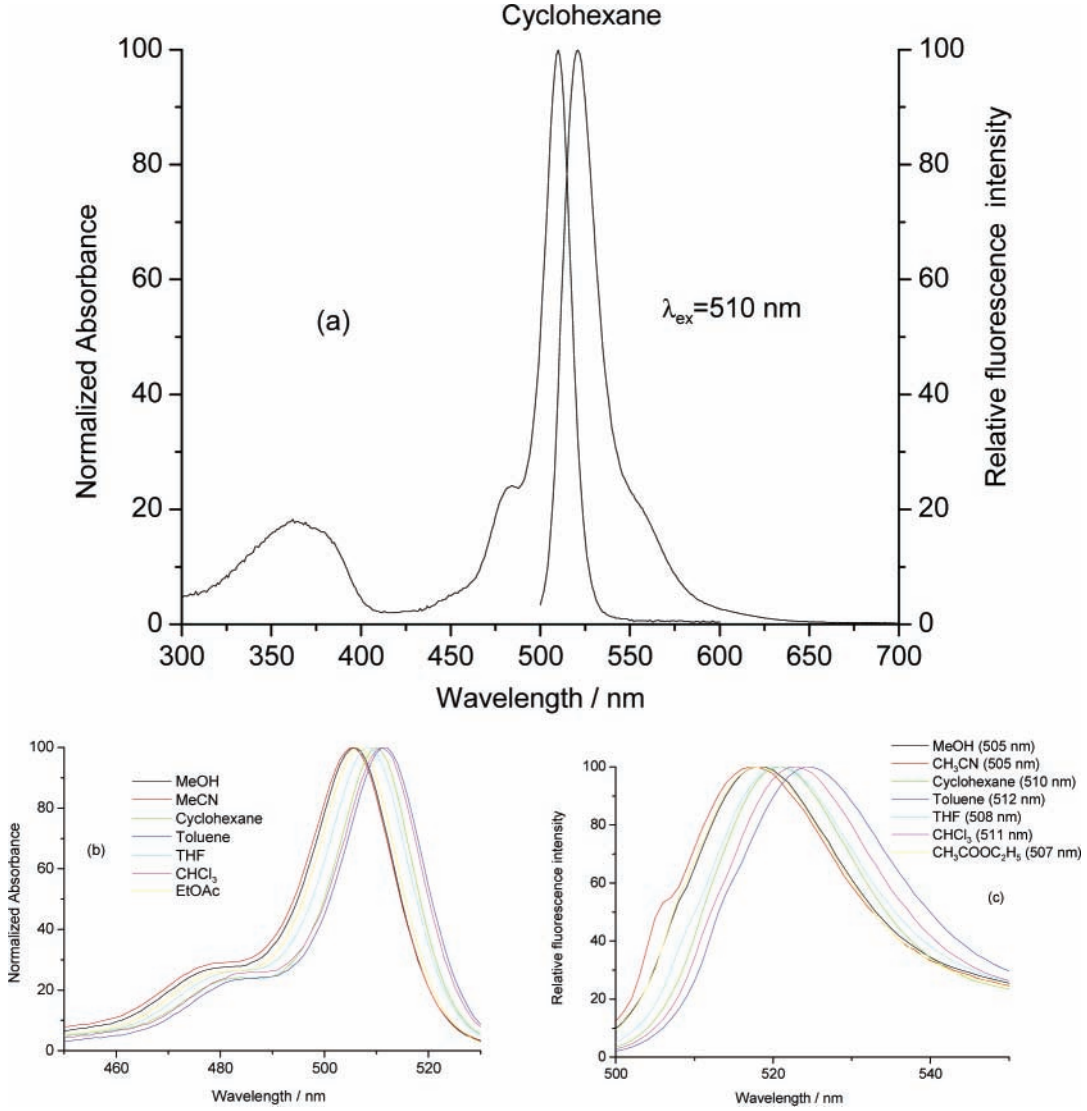

Figure 1. (a) Normalized absorbance and fluorescence emission spectra of **1** in cyclohexane. (b) Enlargement of the main absorbance peak of **1** in several solvents. (c) Enlargement of the main fluorescence emission peak of **1** in several solvents. The excitation wavelengths used in part c are given in parentheses. The intensities in this figure are normalized to the same value at the wavelength of maximum intensity.

has been extended to the case of an *n*/1 complex between cation and indicator (eq 4).[16] The K_a values of the ammonium salts of **5**, **6**, and **7** were determined by fluorimetric titration as a function of pH using the fluorescence excitation and/or emission spectra (at least four independent measurements were used to compute the average K_a value). Nonlinear fitting of eq 4 to the steady-state fluorescence data (F) recorded as a function of $[H^+]$ yields values of K_a, the fluorescence signals F_{min} and F_{max} at minimal and maximal $[H^+]$, respectively (corresponding to the uncharged amine and positively charged ammonium forms of the pH probe, respectively), and n (the number of protons bound per amine). Equation 4 assumes that the absorbance of the sample is small (<0.1) and that the binding of H^+ to the probe in the excited state is negligible.

$$F = \frac{F_{max}[H^+]^n + F_{min}K_a}{K_a + [H^+]^n} \qquad (4)$$

Fitting eq 4 to the steady-state fluorescence data (F) with n, K_a, F_{min}, and F_{max} as freely adjustable parameters always gave values of n close to 1, indicating that one proton is bound per tertiary amine molecule. Therefore, n was kept fixed at 1 in the final curve fittings, from which the estimated values of K_a, F_{min}, and F_{max} are reported here.

Results and Discussion

Spectroscopic Properties of 1, 2, 3, and 4. Figure 1 shows the absorption and steady-state fluorescence emission spectra of **1** dissolved in several solvents. The absorption spectra are of similar shape as those of described BODIPY dyes,[6−8] with a strong absorption band around 500 nm and a shoulder at the short wavelength side. The absorption spectra are only barely affected by solvent polarity, with the maximum being slightly shifted hypsochromically (~7 nm) when the solvent is changed from toluene (512 nm) to acetonitrile (505 nm), which is consistent with the general behavior of BODIPY chromophores.[6−8] This shift reflects the polarizability of the solvent and has also been observed for cyanine dyes[17] and aromatic amines.[18] They all show narrow spectral bandwidths with two absorption maxima: (1) a strong S_0-S_1 transition with a maximum appearing at 509 ± 4 nm and (2) the second maximum, or shoulder on the high energy side, centered at about 480 nm, which is attributed to the 0−1 vibrational transition. The molar absorption coefficients (ϵ) for the new BODIPY analogues are relatively high and lie in the 21 000−65 000 M^{-1}

TABLE 1: Photophysical Properties of BODIPY Compounds 1, 2, 3, and 4 in Several Solvents

BODIPY	solvent	λ_{abs} (max/nm)	λ_{em} (max/nm)	λ_{ex} (max/nm)	fwhm$_{abs}$ (cm^{-1})	$\Delta\bar{\nu}$ (cm^{-1})	ϕ_f	τ (ns)	k_f (10^9 s^{-1})	k_{nr} (10^9 s^{-1})
1	toluene	512	524	512	806	447	0.52	3.35	0.16	0.14
	$CHCl_3$	511	523	511	769	449	0.46	3.28	0.14	0.16
	cyclohexane	510	521	510	695	414	0.42	2.87	0.15	0.20
	THF[a]	508	521	508	775	491	0.36			
	EtOAc	507	518	506	781	419	0.30	2.24	0.13	0.31
	MeOH	506	518	505	785	458	0.25	1.87	0.13	0.40
	MeCN	505	517	505	825	460	0.21	1.60	0.13	0.49
2	toluene	513	528	513	836	554	0.42	2.65	0.16	0.22
	$CHCl_3$	513	526	513	803	482	0.38	2.65	0.14	0.23
	cyclohexane	512	524	512	766	447	0.29	1.94	0.15	0.37
	THF[a]	510	525	510	809	560	0.25			
	EtOAc	508	522	508	775	528	0.25	1.71	0.15	0.44
	MeOH	508	521	508	819	491	0.19	1.46	0.13	0.56
	MeCN	507	521	507	819	530	0.17	1.33	0.13	0.63
3	toluene	517	538	517	898	755	0.12	0.82	0.15	1.07
	$CHCl_3$[a]	517	538	517	863	755	0.095			
	cyclohexane	515	533	515	869	656	0.073	0.54	0.13	1.71
	THF	514	536	514	949	799	0.056			
	EtOAc	512	533	511	960	770	0.053			
	MeOH	511	533	511	960	808	0.032			
	MeCN	511	531	511	1000	739	0.039			
4	toluene	519	543	518	930	852	0.076	0.55	0.14	1.68
	$CHCl_3$	519	543	518	930	852	0.055			
	cyclohexane	517	539	517	898	789	0.038			
	THF	516	540	515	1056	861	0.037			
	EtOAc	513	537	513	989	871	0.035			
	MeOH	513	538	513	992	906	0.026			
	MeCN	512	537	512	992	909	0.030			

[a] The fluorescence decays measured as a function of emission wavelength could only be described globally by a triple-exponential decay law.

cm^{-1} range. In addition, a considerably weaker, broad absorption band is found at about 375 nm for **1**, and its position is not appreciably affected by solvent polarity. We attribute this broader and weaker absorption band to the S_0-S_2 transition. Table 1 summarizes the photophysical data of compounds **1**−**4** in several solvents.

Compound **1** also shows the typical emission features of BODIPY[6−8] (Figure 1), that is, a narrow, slightly Stokes-shifted band of mirror image shape, a high fluorescence quantum yield (ϕ_f) which decreases (from 0.52 in toluene to 0.21 in acetonitrile) with increasing solvent polarity, and fluorescence bands that are hypsochromically shifted (from 524 nm in toluene to 517 nm in acetonitrile) with increasing solvent polarity and decreasing polarizability. The linearity of a plot of the absorption ($\bar{\nu}_{abs}$) and fluorescence ($\bar{\nu}_{em}$) maxima versus $f(n^2) = (n^2 - 1)/(2n^2 + 1)$ (Figure 2) confirms that van der Waals interactions with a polarizable solvent can rationalize the solvent dependence of the excitation energy. If a large difference in permanent dipole moment would exist between the ground and excited state, the excitation energy would depend linearly on $f(\epsilon) - f(n^2) = [(\epsilon - 1)/(2\epsilon + 1)] - [(n^2 - 1)/(2n^2 + 1)]$ rather than on $f(n^2)$, and hence, no linear dependence on $f(n^2)$ would be observed anymore (e.g., the data points for chloroform and toluene would be situated between those of tetrahydrofuran and cyclohexane). Also, the independence of the Stokes shift upon the solvent polarity (Table 1) indicates that the permanent dipole moments (if any) do not differ between the ground state and the excited state.[19] The absorption and emission spectra display perfect mirror symmetry, showing that the main bands correspond to the S_0-S_1 transition. The fluorescence decay profiles of **1** could be described by a single-exponential fit (fluorescence lifetimes (τ) in the 1.60−3.35 ns range) in all of the solvents investigated except for tetrahydrofuran (THF). In fact, the radiative rate constant $k_f = (0.14 \pm 0.01) \times 10^9$ s^{-1} is identical within experimental error (Table 1). These values suggest that the oscillator strength is close to 1, corresponding to the large extinction coefficients. The fluorescence quantum yield (ϕ_f) and lifetime (τ) decrease when the solvent changes from toluene (0.52 and 3.35 ns) to acetonitrile (0.21 and 1.60 ns), due to an increase of the nonradiative rate constant (k_{nr}) in more polar solvents. The S_1-S_0 transition of BODIPY compounds **1**−**4** resembles strongly that of cyanine dyes. This is no surprise, as the "core" of the molecule consists of an extended delocalized π-system with two completely equivalent delocalized structures A and B (Figure 3a), leading to the absence of bond alternation. Single-crystal X-ray structural analysis of fused BODIPY analogues has shown that the average bond length of N3a−C3 and N4a−C5 indicates a pronounced double-bond character in contrast to the average bond length of N3a−C8a and N4a−C7a, which is significantly longer.[20] Nonetheless, a strong π-electron delocalization is observed within the central six-membered ring and both adjacent five-membered rings. This π-electron delocalization is interrupted between both B−N bonds. For symmetry reasons, all ring atoms of the BODIPY chromophore are exactly positioned within a plane. Although BODIPY resembles monomethine cyanines where the delocalization involves 6 π-electrons distributed over 5 atoms, closer inspection shows that the actual chromophore consists of 12 π-electrons distributed over 11 atoms, which makes it isoelectronic with heptamethine cyanines.

The absorption and emission spectra of **2**, **3**, and **4** are, in general, similar to those of **1** in the solvents used. Both the long wavelength absorption band and the fluorescence band are bathochromically shifted when the polarizability of the solvent is increased.

Figure 4 shows the absorption and fluorescence spectra of **1**, **2**, **3**, and **4** in methanol. A slight bathochromic shift appears to increase with increasing electron withdrawing power of the *para*-substituent (R) (see Scheme 1) in the phenyl group. Indeed, the hydrogen group (in **2** vs the methoxy group in **1**) causes a spectral shift to the red of 2 and 3 nm in the absorption and fluorescence bands, respectively, whereas the carbomethoxy

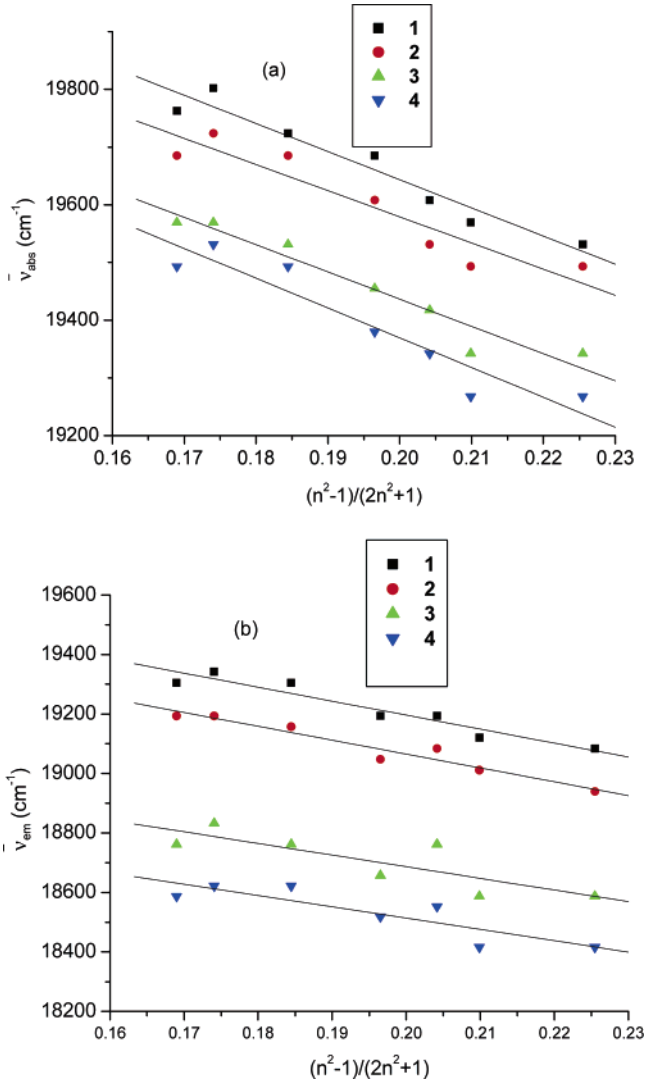

Figure 2. Plots of the absorption maxima ($\bar{\nu}_{abs}$) (a) and fluorescence emission maxima ($\bar{\nu}_{em}$) (b) for compounds **1**−**4** vs $(n^2 - 1)/(2n^2 + 1)$ as a function of solvent. From left to right: MeOH, MeCN, EtOAc, THF, cyclohexane, $CHCl_3$, and toluene.

group (**3** vs **1**) gives rise to a larger corresponding shift of 5 and 15 nm to lower energies in the absorption and fluorescence spectra, respectively. The cyano group (in **4**) causes an even larger bathochromic shift of 7 and 20 nm in the absorption and emission bands, respectively, compared to compound **1**. Similar small bathochromic shifts that increase with the electron withdrawing strength of the *para*-substituent (R) in compounds **1**−**4** are observed in the other solvents. In all cases, the shifts are smaller in absorption than in emission. The fact that the absorption and emission bands show a bathochromic shift with increasing electron withdrawing tendency of the *para*-substituent (R) can be rationalized as follows. Ab initio and semiempirical calculations indicate that the S_0-S_1 transition is a nearly pure highest occupied molecular orbital (HOMO)−lowest unoccupied molecular orbital (LUMO) transition.[8] The electron density map of these states suggests an important increase in the electronic density at position 8 in the LUMO with respect to the HOMO state. The higher the electron withdrawing ability of the *para*-substituent (R), the better the LUMO is stabilized. On the other hand, the substituent in position 8 will have little influence on the HOMO, as the latter orbital has a node at this position. Hence, an electron withdrawing group in position 8 will decrease the HOMO−LUMO energy difference. The time-resolved

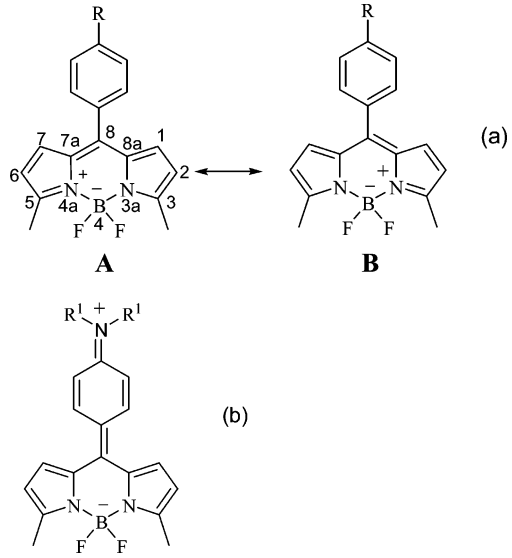

Figure 3. (a) The two main delocalized structures of the BODIPY fluorophore, including the numbering. (b) Representation of the CT excited state of compounds **5**−**7**.

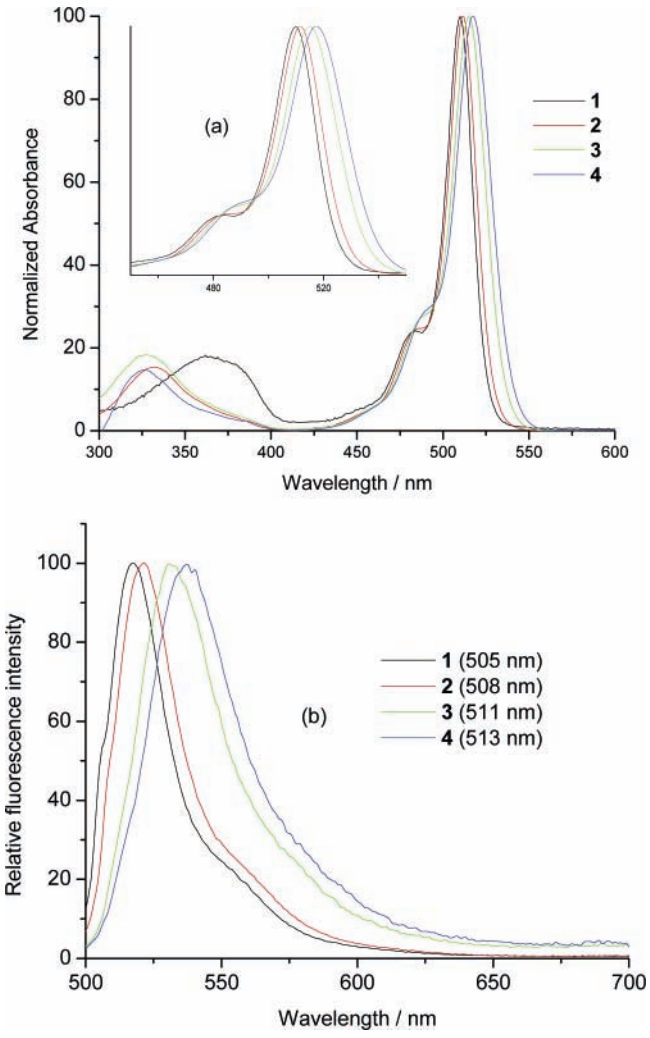

Figure 4. Normalized absorbance (a) and fluorescence emission (b) of **1**, **2**, **3**, and **4** in methanol. The intensities are normalized to the same value at the wavelength of maximum intensity. The inset shows an enlargement of the main peak. The excitation wavelengths used in part b are given in parentheses.

emission of **2**, **3**, and **4** can be described by a monoexponential decay function in most solvents. In the same solvent, the ϕ_f

and τ values decrease with increasing electron withdrawing strength of the *para*-substituent (R) (Table 1), which is due to a faster nonradiative decay rather than to a slower radiative decay. Indeed, the experimental results indicate that the *para*-substituent (R) in **2**, **3**, and **4** does not lead to a significant change in the value of k_f, in analogy to **1**. Although both the fluorescence quantum yield (ϕ_f) and lifetime (τ) are highest for **1**, the radiative rate constants remain the same [$k_f = (0.14 \pm 0.01) \times 10^9$ s^{-1}] for **1**−**4**, irrespective of the nature of the solvent. The nonradiative rate constants (k_{nr}), however, decrease in going from **4** to **1** according to **4** > **3** > **2** > **1**.

The Stokes shift ($\Delta\bar{\nu}$), calculated from the wavelengths of maximum intensity, also increases as with the electron withdrawing strength of the *para*-substituent (R). The Stokes shifts measured for **4** are 2 times larger than those for **1**. Moreover, the Stokes shifts of each compound do not vary much as a function of the solvent. This suggests that increasing the electron withdrawing properties would lead to larger geometric rearrangements upon excitation. This increased electron phonon coupling could also be responsible for the increased nonradiative decay. A possible candidate for the vibration responsible for the electron phonon coupling could be the rotation of the phenyl which becomes more coplanar upon excitation, with the effect being most outspoken for electron withdrawing groups in the *para* position.

To conclude, although the photophysical properties of compounds **1**−**4** resemble strongly those of cyanine dyes, they have the advantage that the difluoroboron bridge avoids the cis−trans isomerism associated with cyanine dyes absorbing in the same spectral regions and leads in apolar solvents to significantly higher quantum yields.[17,21] The smaller extinction coefficient and oscillator strength compared to cyanines dyes with the same number of π-electrons in the polymethine chain can be attributed to the folding of this polymethine chain, leading to a smaller transition dipole. Another difference with cyanine dyes is the presence of a second absorption band 7000−10 000 cm^{-1} above the S_0-S_1 transition. For the latter transition, which will be discussed more in detail when discussing compounds **5**−**7**, a bathochromic shift was induced by the electron donating methoxy group in the *para* position.

Spectroscopic Properties of 5, 6, and 7. The steady-state absorption and fluorescence emission spectra of **5**, **6**, and **7** are depicted in Figures 5, 6, and 7, respectively. The absorption spectra of **5**−**7** are apparently almost the same as those of **1**−**4** (with the exception of a wider base) and are identical with the well-known absorption pattern for BODIPY derivatives.[6−8] In compounds **5**−**7**, a strong S_0-S_1 transition with a maximum around 500 nm and a shoulder at a shorter wavelength is observed, while the intensity of the absorption band around 350 nm is strongly diminished. The molar absorption coefficients for BDP derivatives **5**−**7** are relatively high and lie in the 52 000−95 000 M^{-1} cm^{-1} range. While the absorption maxima show the same solvent dependence as those of compounds **1**−**4**, closer inspection shows the presence of a tail at the red edge of the first absorption band in solvents more polar than toluene for **5** and **6**, which becomes the most outspoken in the most polar solvents acetonitrile and methanol. The red shift of the whole spectrum including the tail in toluene is due to increased polarizability. The occurrence of the red tail in more polar solvents is at the expense of the band observed at 425 nm in cyclohexane and 450 nm in toluene. For **7**, the appearance of the red tail is less clear. This was not observed for compounds **1**−**4**. Taking into account the red shift of the S_0-S_2 transition upon introduction of the electron donating *p*-methoxy group, one cannot exclude that the weaker S_0-S_2 transition is now overlapping with the vibronic progression of the S_0-S_1 transition. As the former is characterized by a relatively wide and structureless band, the general effect will be—agreeing with our observations—an increase of the extinction coefficient of the first absorption band. Due to the strong overlap with the S_1-S_0 transition, the maximum of this second band which corresponds to the energy of the Franck−Condon charge transfer (CT) state (cfr. infra) is for **5** and **6** hidden under the intense S_0-S_1 transition, and hence, its maximum cannot be determined accurately. Therefore, we only observe the red tail of the CT absorption band. There is no indication that in the solvents used here the energy of this Franck−Condon CT state is lower than that of the cyanine-like excited state.

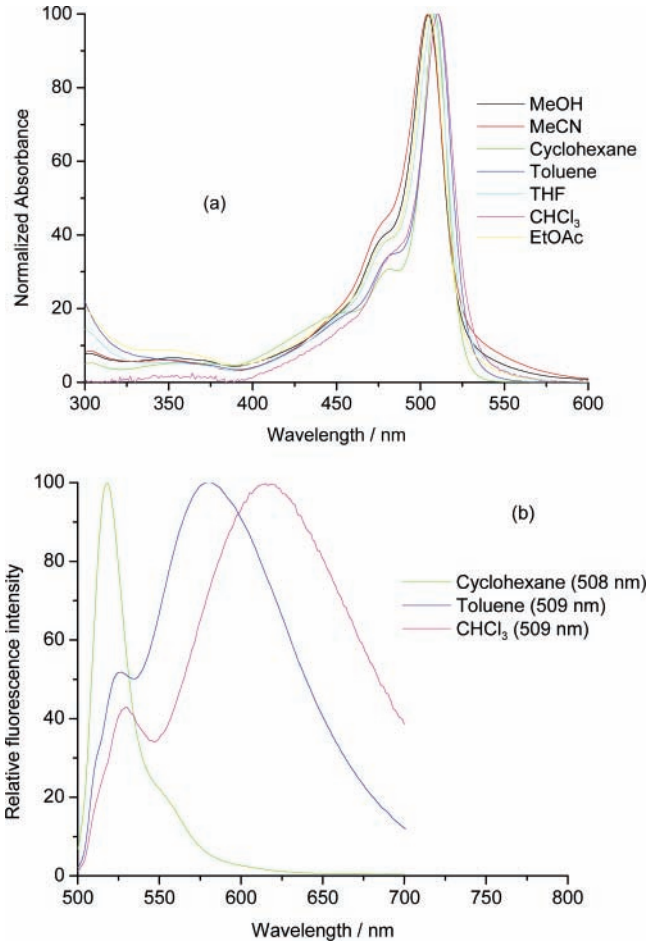

Figure 5. Normalized absorbance (a) and fluorescence emission (b) of **5** in several solvents. The intensities are normalized to the same value at the wavelength of maximum intensity. The excitation wavelengths used in part b are given in parentheses.

Furthermore, the emission behavior of **5**−**7** is strongly solvent dependent. In cyclohexane, BODIPY analogues **5**−**7** show emission at about 520 nm shaped like the mirror image of the absorption spectrum. In cyclohexane, the emission spectra of **5**−**7** strongly resemble those of **1**−**4**. In analogy to **1**−**4**, the emission can be attributed to the polymethine chromophore, also responsible for the lowest energy intense absorption band. The excited state to which this emission can be attributed will be called the LE state. In all solvents more polar than cyclohexane, however, this LE emission is (strongly) quenched and the formation of a second broad emission band is observed at longer wavelengths.

With increasing solvent polarity, the intensity of the long wavelength emission band decreases, while the maximum of

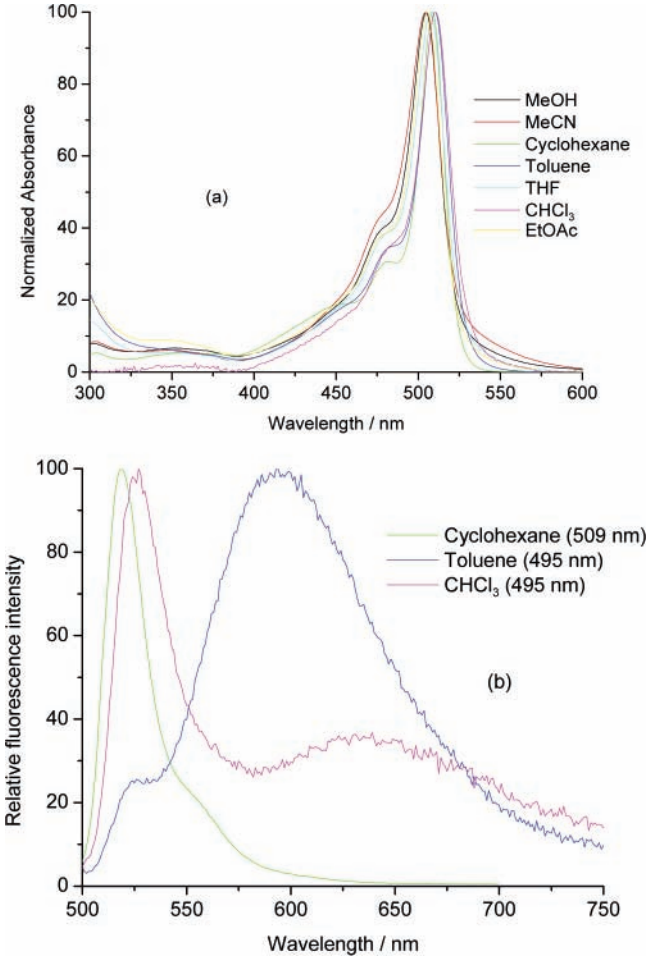

Figure 6. Normalized absorbance (a) and fluorescence emission (b) of **6** in several solvents. The intensities are normalized to the same value at the wavelength of maximum intensity. The excitation wavelengths used in part b are given in parentheses.

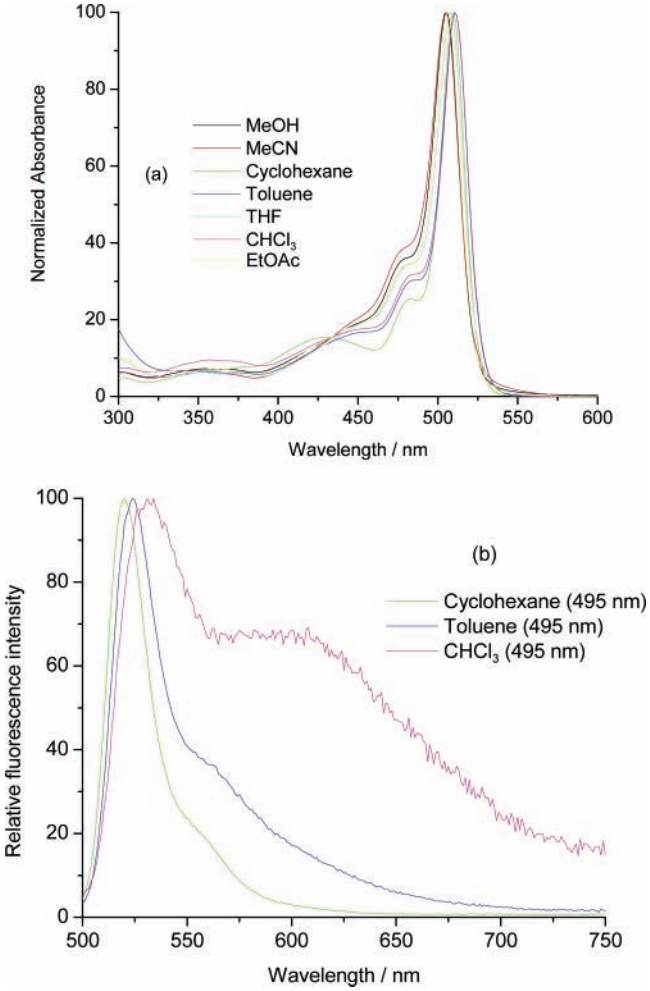

Figure 7. Normalized absorbance (a) and fluorescence emission (b) of **7** in several solvents. The intensities are normalized to the same value at the wavelength of maximum intensity. The excitation wavelengths used in part b are given in parentheses.

the band shifts more to the red. In acetonitrile, methanol, and ethyl acetate, this broad bathochromic emission has such a low intensity that it can hardly be detected. This red-shifted band occurs at longer wavelengths for **5** and **6** compared to **7**. More quantitative experiments show that the quantum yield of fluorescence (ϕ_f) in aerated solutions decreases with increasing polarity of the solvent from cyclohexane to acetonitrile. The ϕ_f values were also determined in deaerated solutions of cyclohexane, toluene, and chloroform and are within experimental error about the same as those in the corresponding aerated solutions. This is to be expected because the fluorescence lifetimes are rather short (see next paragraph), so that oxygen quenching will have a limited effect. Table 2 summarizes the photophysical data of BODIPY analogues **5**−**7** in several solvents.

The solvent dependence of the long wavelength emission points to an excited state with a large dipole. This can also clarify why a broad bell shaped structureless band is observed. The CT excited state may be represented by the delocalized structure depicted in Figure 3b.

The same CT state will also be responsible for the short wavelength absorption band observed for **1**−**4** in all solvents and for **5**−**7** in cyclohexane. This clarifies why this transition shifts to longer wavelengths from **2**−**4** over **1** to **5**−**7** according to the electron donating character of the *para*-substituent (R). This CT state is at lower energy in **5** and **6** compared to **7**, as indicated by the more prominent red tail in the absorption spectrum and the larger red shift of the fluorescence spectrum (Figures 5−7). In the absorption spectrum of **7**, the absorption spectrum of the CT state is mainly hidden under that of the LE state (Figure 7a).

Increasing the solvent polarity also leads to a more prominent red tail in the absorption spectrum. This indicates that the transition to the CT state shifts to lower energy upon increasing the solvent polarity. The dependence of the absorption maximum on the solvent polarity is given by

$$\bar{\nu}_{abs} - \bar{\nu}^0_{abs} = \frac{2(\mu_G - \mu_E)}{4\pi\epsilon_0 hc\rho^3}\left[\frac{\mu_G(\epsilon - 1)}{2\epsilon + 1} - \frac{(\mu_G - \mu_E)(n^2 - 1)}{2(2n^2 + 1)}\right] \quad (5)$$

$\bar{\nu}_{abs}$ and $\bar{\nu}^0_{abs}$ correspond to the absorption maximum (cm^{-1}) in a solvent with dielectric constant ϵ and refractive index n and the absorption frequency in a vacuum, respectively. ϵ_0, h, c, and ρ correspond to the permittivity of a vacuum (8.85×10^{-12} C V^{-1} m^{-1}), Planck's constant (6.6×10^{-34} J s), the velocity of light in a vacuum (3.0×10^{10} cm s^{-1}), and the radius of the solvent cavity (in m), respectively. μ_E (C m) and μ_G (C m) are the permanent dipole moments of the ground state and the excited state, respectively. The first term in eq 5 indicates that the position of the absorption band can depend only on $f(\epsilon)$ when μ_G differs from zero. Hence, the red shift of the absorption

TABLE 2: Photophysical Properties of BODIPY Compounds 5, 6, and 7 in Several Solvents

BODIPY	solvent	λ_{abs} (max/nm)	λ_{em} (max/nm)	λ_{ex} (max/nm)	fwhm$_{abs}$ (cm^{-1})	ϕ_f[a]	ϕ_f[b]	τ_1 (ns)	τ_2 (ns)	k_f (10^9 s^{-1})	k_{nr} (10^9 s^{-1})
5	toluene	509	580	509	934	0.15	0.15	0.028	3.24		
	$CHCl_3$[a]	509	615	509	1136	0.058	0.094				
	cyclohexane	508	518	508	741	0.37	0.37	2.72		0.14	0.23
	THF	506			1024	0.002					
	EtOAc	505			991	0.004					
	MeOH	504			1159						
	MeCN	503			1329						
6	toluene	511	593	509	890	0.13	0.16	0.015	3.12		
	$CHCl_3$[a]	511	527	511	981	0.077	0.090				
	cyclohexane	509	519	508	738	0.33	0.33	2.31		0.14	0.29
	THF	507	527	508	979	0.01					
	EtOAc	506			945	0.006					
	MeOH	505			991	0.005					
	MeCN	504			1196	0.003					
7	toluene	511	524	510	769	0.32	0.35	0.028	3.12		
	$CHCl_3$[c]	511	531	513	809	0.11	0.10				
	cyclohexane	509	520	509	695	0.35	0.35	2.15		0.16	0.30
	THF	507	695	507	897	0.013					
	EtOAc	506			825	0.008					
	MeOH	505			866	0.005					
	MeCN	504			949	0.002					

[a] ϕ_f values determined for aerated samples. [b] ϕ_f values determined for degassed samples (freeze−pump−thaw cycles). [c] The fluorescence decays measured as a function of emission wavelength could only be described globally by a triple-exponential decay law.

maximum of the transition to the CT state with increasing $f(\epsilon)$ suggests that the ground-state dipole will not be zero and hence that the polar delocalized structure also contributes to the ground state. It is however insufficient to shift the Franck−Condon excited state of the CT transition below that of the LE transition, even in polar solvents.

Under those conditions, the Franck−Condon LE state will be, even for the *p*-aminosubstituted benzenes **5**−**7** in polar solvents, below the CT state and the lowest absorption band will always have a predominant LE character. However, when after excitation this CT state is reached, it will be stabilized in solvents more polar than cyclohexane to an extent that its energy becomes lower than that of the LE, and intramolecular conversion from the LE to the CT state will occur. Hence, compounds **5**−**7** show dual emission.[22]

Due to the large dipole moment difference between the CT excited state and the ground state, electron phonon coupling with solvent phonons, which can act as accepting modes for internal conversion, will become increasingly important in polar solvents, leading to a faster decay of the fluorescence.[23]

In cyclohexane, the emission of **5**−**7** decays monoexponentially, yielding radiative rate constants of similar magnitude [$k_f = (0.14 \pm 0.01) \times 10^9$ s^{-1}]. This value for k_f was also found for **1**−**4**. The nonradiative rate constant values (k_{nr}) are slightly higher than those for compound **1**. This again suggests that in cyclohexane the excited state of **5**−**7** is a pure LE state. In toluene, the fluorescence decays of **5**−**7** could only be described globally by a biexponential decay law with τ_1 being in the 15−28 ps range (fast component) and τ_2 being about 3.2 ns (slow component). The time-resolved fluorescence profiles of **5** in toluene were measured as a function of emission wavelength (λ_{em} = 525, 550, 570, and 600 nm) and analyzed globally as biexponentials with linked decay times τ_1 (fast) and τ_2 (slow). Measurements of fluorescence decay traces as a function of λ_{em} in the region 525−600 nm revealed a decrease of the relative amplitude associated with the fast component (τ_1) with increasing detection wavelength (λ_{em}). Indeed, the ratio of the pre-exponential factors (α_1/α_2) decreases with increasing λ_{em} (α_1/α_2 = 5.176 at 525 nm, α_1/α_2 = 1.284 at 550 nm, and α_1/α_2 = 0.276 at 570 nm) and even becomes negative at the longest emission wavelength ($\alpha_1/\alpha_2 = -0.198$ at 600 nm). At shorter observation wavelengths (λ_{em}), the emission originates mainly from the LE state, whereas, at longer λ_{em}, primarily the CT state emission is observed (see emission spectra of Figure 5b). This is consistent with a mechanism involving the excitation of a single ground-state species to a LE state followed by a fast conversion to a CT state. According to such a kinetic model, the ratio α_1/α_2 should be −1 under conditions where the LE is excited exclusively and only emission from the CT state is observed.[24] This is not yet the case at λ_{em} = 600 nm, which can be due to either observation of LE emission at 600 nm and/or direct excitation of the CT state at 488 nm. Actually, the absorption spectra suggest that for **5**−**7** the transition to the CT state is hidden below that of the LE transition. If the conversion from the LE to the CT state is irreversible, the short decay time (τ_1) can be considered as the lifetime of the LE state which is substantially shortened by the new decay channel opened. Under those conditions, the slow decay time (τ_2) can be attributed to the lifetime of the CT state. If the interconversion is reversible, the interpretation of the decay times is more complex and a complete analysis generally requires prior knowledge of the fraction of the excitation leading to LE and CT as well as of the fraction of the emission due to the LE and CT states or some a priori knowledge of some rate constants.[24,25] Figure 8 displays the fluorescence decay traces at λ_{em} = 525 nm and at λ_{em} = 600 nm. The curve at 525 nm is clearly a sum of two exponentials, while the curve at 600 nm is a difference of two exponentials. The ratio of the pre-exponential factors (α_1/α_2) for compound **6** in toluene also decreases with increasing emission wavelength (λ_{em}) (α_1/α_2 = 16.38 at 525 nm, α_1/α_2 = 3.336 at 550 nm, α_1/α_2 = 1.376 at 570 nm, and α_1/α_2 = 0.010 at 600 nm). For compound **7** in toluene, the variation of α_1/α_2 (α_1/α_2 = 1.087 at 510 nm, α_1/α_2 = 1.084 at 520 nm, α_1/α_2 = 1.054 at 530 nm, and α_1/α_2 = 0.905 at 540 nm) as a function of λ_{em} is not as large as that for **5** and **6** in toluene. The small dependence of α_1/α_2 on λ_{em} for **7** compared to **5** and **6** is to be expected on the basis of their fluorescence emission spectra (Figures 5b, 6b, and 7b). In the absorption and emission spectra, the red tail and shifted band are less pronounced for compound **7** compared to compounds **5** and **6**.

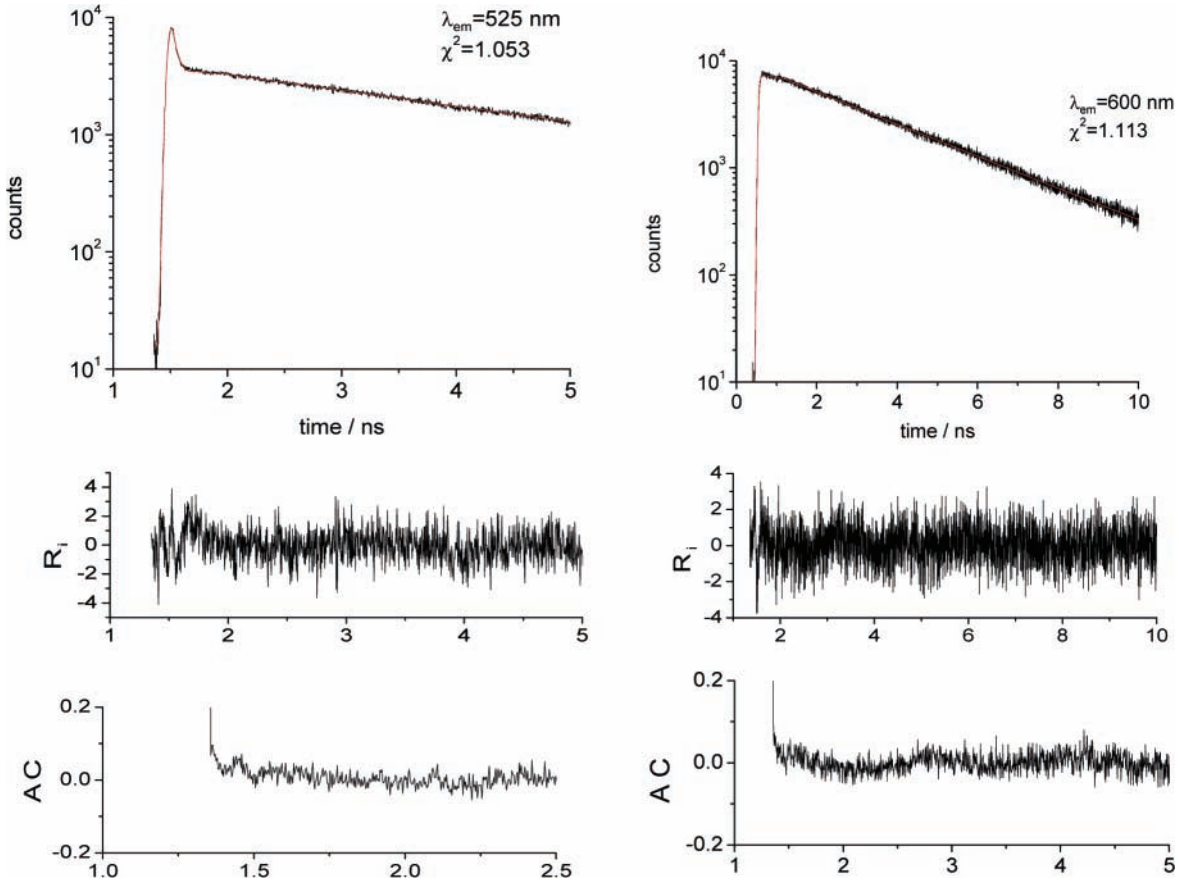

Figure 8. (left) Experimental fluorescence decay curve (black) of **5** in toluene ($\lambda_{ex} = 488$ nm, $\lambda_{em} = 525$ nm). The best fit (red) via global analysis with decay times τ_1 and τ_2 linked over the observation wavelengths (λ_{em}) ($\chi_g^2 = 1.094$) yielded $\tau_1 = 28$ ps and $\tau_2 = 3.24$ ns with $\alpha_1 = 12.667$ and $\alpha_2 = 2.447$. (right) Experimental fluorescence decay curve (black) of **5** in toluene ($\lambda_{ex} = 488$ nm, $\lambda_{em} = 600$ nm). The best fit (red) via global analysis yielded $\alpha_1 = -0.52$ and $\alpha_2 = 2.622$. Also given are the local reduced χ^2 values, the weighted residuals (R_i), and the autocorrelation functions (AC).

Fluorimetric Titrations of 5, 6, and 7. In **5**−**7**, the intramolecular charge transfer (ICT) can be efficiently blocked by protonation. In aqueous solution, the effect of protonation on the emission behavior of **5**−**7** is very large. Protonation turns the BODIPY derivatives into highly fluorescent molecules, the CT emission disappears, and the emission from the LE state with its characteristically higher fluorescence quantum yield is re-established. Now, we will examine the spectral changes of **5**−**7** upon protonation in aqueous (nonbuffered) solution.

Absorption Spectra. The absorption spectra of **5**−**7** show interesting changes as a function of pH. From Figure 9a, it is evident that varying the pH gives rise to several isosbestic points and is accompanied by a hypsochromic shift of the major absorption maximum of **5** (from 494 nm at pH 1.09 to 473 nm at pH 8.60) upon increasing the pH. This blue shift of the major maximum at higher pH, which will be commented on later, is accompanied by the appearance of a clear shoulder around 550 nm, which is attributed to a transition to the CT state. Upon protonation of the aniline moiety, the CT state shifts to higher energy, as indicated by the appearance of a band with a maximum at 350 nm, in analogy to **2**. This band increases with decreasing pH. Upon closer inspection of the spectra, one can see that the transition with a maximum at 494 nm and which is predominant at low pH is much broader than the absorption band of the LE transition in **1**−**4**. The red shift of the CT state of **5** in water is large enough to manifest itself as a separate shoulder rather than as a red tail in the less polar and hydrogen bond donating methanol (Figure 5a for **5**). As the dipolar solvating powers of water and polar organic solvents such as acetonitrile—described by $f(\epsilon)$—are nearly identical, these results indicate that hydrogen bond formation plays a large role in the stabilization of the CT state. For **1**−**4**, it also was found that the major LE transition undergoes a hypsochromic shift when going to the more polar and less polarizable solvents acetonitrile and methanol (see Figure 2) in accordance with their decreased polarizability. From Figure 9a, it is evident that the absorption spectra of the neutral amine and the positively charged ammonium species overlap considerably.

While at low pH the absorption band at 494 nm can be attributed to the LE transition of BODIPY with a protonated aniline nitrogen, this band shifts to 473 nm at high pH where the aniline nitrogen is no longer protonated. This shift is in agreement with the substituent effects observed for **1**−**4** because the LUMO of the BODIPY chromophore is destabilized by interacting in position 8 with the electron rich aniline moiety.

Analogous effects are found for **6**, where the major absorption maximum shifts hypsochromically from 493 nm at pH 1.12 to 484 nm at pH 7.85. The CT band of the tertiary amine has a maximum around 550 nm and shifts upon protonation to higher energy, as indicated by the appearance of a band with a maximum around 340 nm. While in acetonitrile and methanol the transition to the CT state of **6** is only visible as a red tail of the major band (Figure 6a), this transition is shifted sufficiently to lower energy in water to give rise to a separate shoulder.

The absorption spectrum of compound **7** as a function of pH is shown in Figure 10a and indicates that the absorption maximum of **7** remains located at 487 ± 1 nm as a function of pH. The CT band of **7** in the studied solvents remains largely

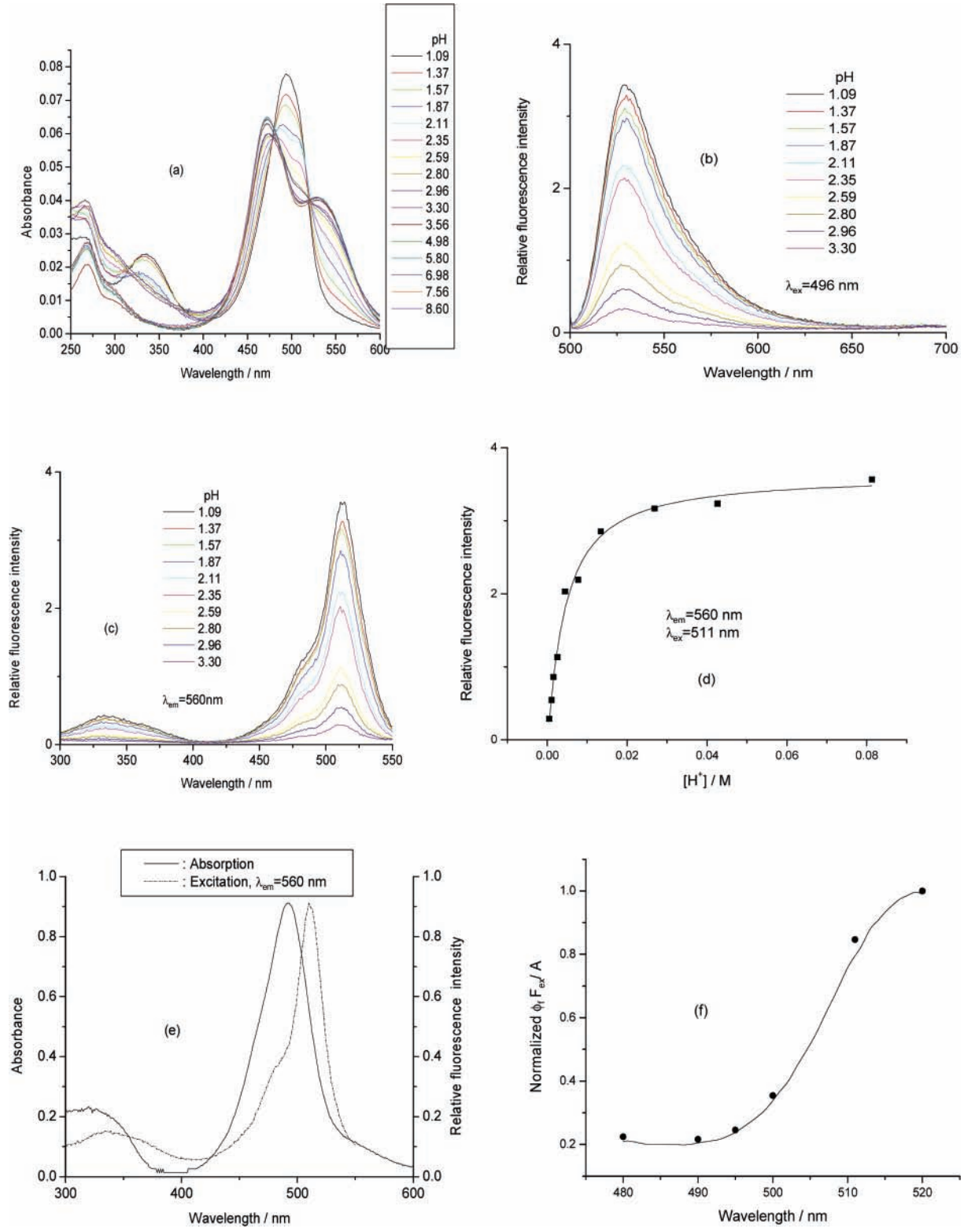

Figure 9. Absorption spectra (a), fluorescence emission spectra (λ_{ex} = 496 nm) (b), fluorescence excitation spectra (λ_{em} = 560 nm) (c), and fluorescence titration curve (d) of **5** in aqueous nonbuffered solution as a function of pH. The solid line in Figure 9d represents the best fit of eq 4 with $n = 1$ to the fluorimetric titration data of **5** obtained from the excitation spectra (Figure 9c, λ_{em} = 560 nm, λ_{ex} = 511 nm). Part e shows normalized absorption and excitation spectra of **5** at pH 1.15, and part f shows the excitation wavelength dependence of ϕ_f of **5** at pH 1.15. The symbols in Figure 9f represent the experimental apparent ϕ_f values, and the solid line is the ratio of the fluorescence excitation signal over the absorbance (F_{ex}/A). The data in Figure 9f are normalized to 1 at 520 nm.

hidden under the major absorption band (Figure 10a), following the tendency of the absorption spectra of **7** in solvents of different polarities (Figure 7a)

Fluorescence Spectra. The fluorescence emission and excitation spectra of **5** in aqueous nonbuffered solution are shown as a function of pH in parts b and c of Figure 9, respectively. By lowering the pH, the fluorescence signals increase significantly. Unlike their absorption spectra, the fluorescence emission maximum at 529 nm and the excitation maximum at 511 nm remain unchanged while the intensity changes as a function of

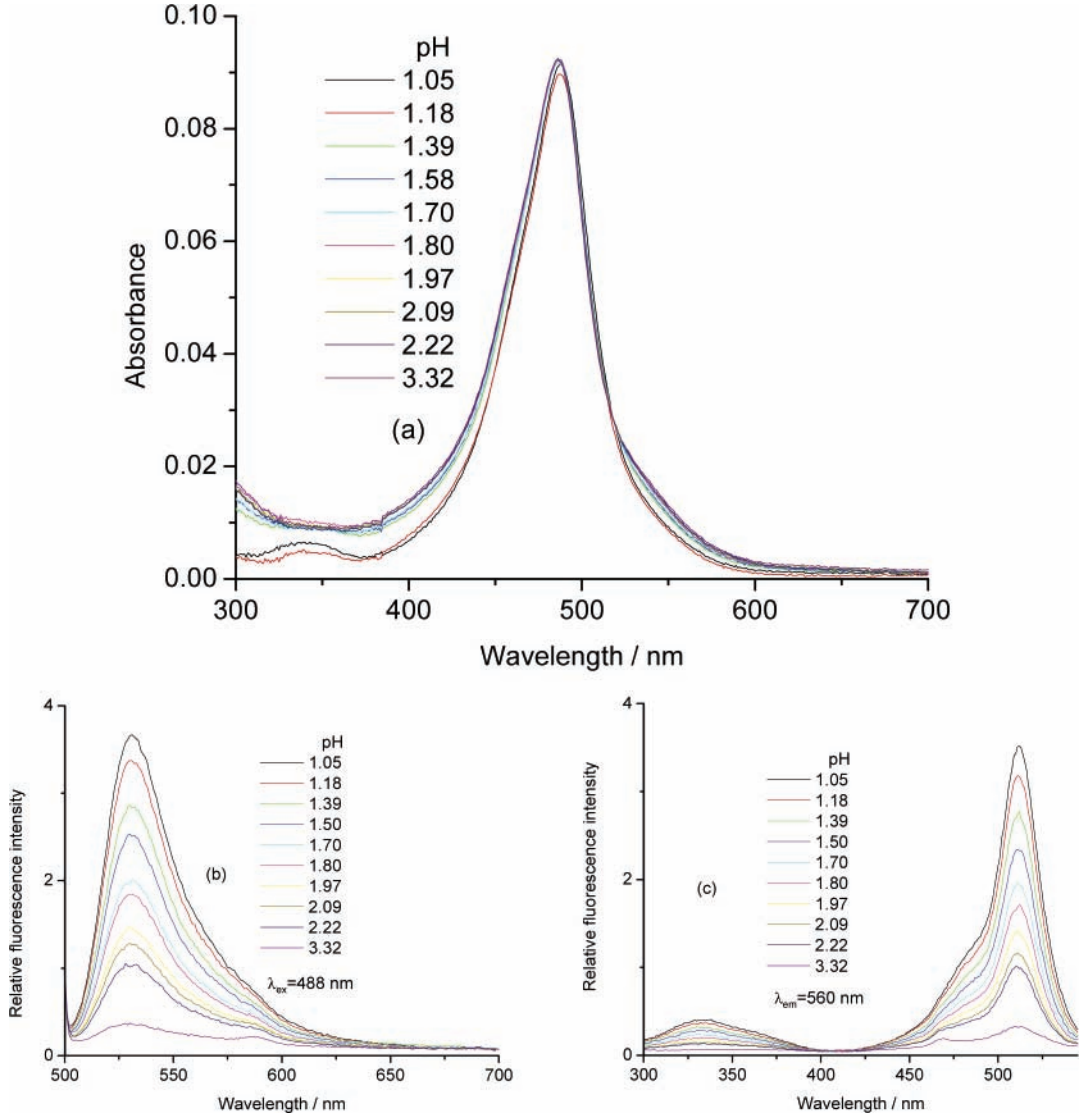

Figure 10. Absorption spectra (a), fluorescence emission spectra ($\lambda_{ex} = 488$ nm) (b), and fluorescence excitation spectra ($\lambda_{em} = 560$ nm) (c) of **7** in aqueous nonbuffered solution as a function of pH.

TABLE 3: Properties of the BODIPY Derivatives in Aqueous Nonbuffered Solution[a]

BDP	$\lambda_{abs-acid}/\lambda_{abs-base}$ (max/nm)	$\lambda_{em-acid}/\lambda_{em-base}$ (max/nm)	ϕ_{f-acid} (pH)	ϕ_{f-base} (pH)	pK_a
5	494/473	529/529	0.03 (1.87)	0.006 (3.3)	2.37 ± 0.06
6	493/484	528/526	0.008 (1.38)	0.001 (4.32)	4.15 ± 0.05
7	488/486	531/528	0.001 (1.05)	0.0002 (3.32)	1.47 ± 0.03

[a] K_a values were determined by fitting eq 4 with $n = 1$ to the fluorescence data. The fluorescence quantum yields ϕ_{f-base} and ϕ_{f-acid} were determined at respectively the highest and lowest pH values (in parentheses) used in the fluorimetric titration. The ϕ_f values of **5**, **6**, and **7** were determined with excitation at 496, 493, and 488 nm, respectively.

pH. The highest ϕ_f value (0.03, determined by excitation at 496 nm, Table 3) is found at low pH (between pH 1.09 and 1.87). At all pH values, the excitation and fluorescence spectra resemble those of compounds **1**−**4**, suggesting that the fluorescence is due to the LE state. At low pH, the amine function is protonated and the phenyl moiety becomes substituted with a weak electron acceptor rather than with an electron donor, leading to an absorption and emission maximum between that of **2** and **3**. When the ammonium group is deprotonated, excitation yields with 100% efficiency an ICT state which is nonfluorescent in water. The absence of pH dependent shifts of the fluorescence excitation and emission bands may be due to the extremely low fluorescence quantum yield of the CT emission in water. This is in agreement with the observations in other solvents where a decrease of ϕ_f of the CT state with increasing solvent polarity is observed. The binding of H^+ by the tertiary amine suppresses the ICT due to ammonium ion formation and hence blocks this nonradiative decay channel of the LE state. This is accompanied by a large fluorescence enhancement.

Compared to **1**−**4**, there are still some discrepancies when the tertiary amine function of **5** is protonated, while the fluorescence excitation (511 nm) and emission (529 nm) maxima of the protonated form of **5** are intermediate between those of **2** and **3** (see Table 1), indicating that **5**−**7** have a similar Stokes shift to that of **1**−**4**. However, the absorption spectrum of the protonated form of **5** is much broader and its maximum (494 nm) is situated between 11 and 25 nm (440−975 cm^{-1}) to

shorter wavelengths compared to the absorption maxima of **1**−**4**. This discrepancy suggests the presence of two different protonated species at low pH. The observation of isosbestic points in the absorption spectra indicates that the ratio between the concentrations of these two species does not change as a function of the pH. While the species which absorbs at 511 nm and emits at 529 nm corresponds to protonation at the aniline nitrogen, the nature of the species absorbing at 494 nm is not clear. The differences between the excitation and absorption spectra (Figure 9e) suggest that both species interconvert only to a limited extent in the excited state. A consequence of the presence of two species is that the measured fluorescence quantum yield (ϕ_f) is only an apparent value because a large part of the incident light is absorbed by the nonfluorescent species with an absorption maximum at 494 nm. Therefore, the apparent ϕ_f values are expected to change as a function of excitation wavelength. It is found experimentally (Figure 9f) that at wavelengths shorter than the maximum of the excitation spectrum the quantum yield values closely follow the ratio of the fluorescence excitation signal over the absorbance. The photophysical behavior of **6** as a function of pH is very similar to that of **5**.

The acidity constant (K_a) and the stoichiometry (n) of the binding of H^+ by the tertiary amine group of compound **5** were determined by fitting eq 4 to the fluorescence excitation or emission spectral data. The results of the fluorimetric titration of **5** using excitation data ($\lambda_{em} = 560$ nm, $\lambda_{ex} = 511$ nm) are displayed in Figure 9d and yield a pK_a value of 2.37 and a well-defined 1:1 stoichiometry between **5** and H^+, indicative of ammonium ion formation. Similar curve fittings were performed to estimate pK_a and n values, using emission spectra at $\lambda_{ex} =$ 496 nm ($\lambda_{em} = 529$, 539, and 549 nm) and excitation spectra at $\lambda_{em} = 560$ nm ($\lambda_{ex} = 501$ and 521 nm). The pK_a values obtained from the emission spectra are 2.46, 2.42, and 2.37, respectively. The corresponding pK_a values from the excitation spectra are 2.37 and 2.24, respectively. These results show that the pK_a values are independent of the wavelengths used. The average estimated pK_a value of the ammonium form of **5** is summarized in Table 3. All estimated n values are indicative of a 1:1 binding between **5** and H^+.

The fluorescence excitation and emission spectra of **6** as a function of pH (between pH 1.12 and 4.32) are analogous to those of **5** shown in parts b and c of Figure 9, respectively. The intensities of the emission (with $\lambda_{max} = 528$ nm) and excitation spectra (with $\lambda_{max} = 511$ nm) increase at lower pH without any appreciable spectral shift. BODIPY analogue **6** has a lower ϕ_f value (0.008 at low pH between 1.12 and 2.93, Table 3) than **5**. The pK_a values obtained from the fluorimetric titrations of **6** indicate that the average estimated pK_a value of the ammonium form of **6** (4.15) is about 1.8 units higher than that measured for **5** (2.37).

Finally, from Figure 10b and c, it is clear that compound **7** does not show any spectral shift upon protonation; there is only an enhancement of the fluorescence emission and excitation intensities with increasing H^+ concentration, as shown for **5**. The fluorescence quantum yield is the lowest of the three studied pH sensitive compounds (0.001 in the pH range from 1.05 to 1.39). The average estimated pK_a value of the ammonium form of **7** is the lowest (1.47). The pK_a values of **6** (pK_a 4.15) > **5** (pK_a 2.37) > **7** (pK_a 1.47) are in accord with the electron releasing effect of the alkyl substituents on the nitrogen of tertiary amines **5**−**7** (piperidino > NMe_2 > morpholino).[26] This clarifies also why the LE transition in the deprotonated form of **7** will be at the longest wavelength of the series **5**−**7** while its CT transition will be at the shortest wavelengths. The BODIPY moiety in the *para* position to the tertiary amine acts as an electron withdrawing unit.

Conclusion

Our study reflects the effect of the *para*-substituent (R) of the phenyl group on the fluorescence properties of BODIPY deriviatives **1**−**4**. The combination of the electron rich *p*-anisol group and the electron deficient BODIPY fluorophore in compound **1** has the highest fluorescence quantum effciency among the four coumpounds. On the other hand, the electron withdrawing *p*-cyano group in derivative **4** produces the smallest ϕ_f value. However, the shape of the absorption and emission spectra is barely affected by changing the *para*-substituent (R).

In polar solvents, the photophysical properties of free (i.e., uncharged) tertiary amines **5**−**7** are governed by a fast interconversion to an ICT state, where the lone electrons of the amine nitrogen are delocalized over the BODIPY, leading to strong quenching of the fluorescence from the LE state. Upon protonation of the amine nitrogen atom, the amine receptor becomes an inductively electron withdrawing group and the ICT process is suppressed, leading to a pH dependent fluorescence enhancement of the LE emission.[7,27] The variation of the *para*-substituent group in compounds **5**−**7** has a large influence on ϕ_f and pK_a. The electron releasing tendency of piperidino > NMe_2 > morpholino is borne out in the pK_a values: **6** (pK_a 4.15) > **5** (pK_a 2.37) > **7** (pK_a 1.47).

Acknowledgment. The authors are grateful to the University Research Fund of the K.U.Leuven for IDO-grant IDO/00/001, GOA 2001/2, and postdoctoral fellowships to W.Q. and M.B. The *Fonds voor Wetenschappelijk Onderzoek*−*Vlaanderen* is thanked for grant G.0320.00. The continuing support through IAP-V-03 is gratefully acknowledged. Ms. A. Stefan is thanked for technical help with the single-photon timing measurements.

References and Notes

(1) (a) Desvergne, J.-P., Czarnik, A. W., Eds. *Chemosensors of Ion and Molecule Recognition*; Kluwer: Dordrecht, The Netherlands, 1997. (b) Haugland, R. P. *Handbook of Fluorescent Probes and Research Chemicals*, 9th ed.; Molecular Probes, Inc.: Eugene, OR, 2002.

(2) Treibs, A.; Kreuzer, F.-H. *Liebigs Ann. Chem.* **1968**, *718*, 208−223.

(3) BODIPY is a registered trademark of Molecular Probes, Inc., Eugene, OR.

(4) (a) Kollmannsberger, M.; Gareis, T.; Heinl, S.; Breu, J.; Daub, J. *Angew. Chem., Int. Ed. Engl.* **1997**, *36*, 1333−1335. (b) Karolin, J.; Johansson, L. B.-Å.; Strandberg, L.; Ny. T. *J. Am. Chem. Soc.* **1994**, *116*, 7801−7806. (c) Pavlopoulos, T. G.; Shah, M.; Boyer, J. H. *Appl. Opt.* **1988**, *27*, 4998−4999. (d) Johnson, I. D.; Kang, H. C.; Haugland, R. P. *Anal. Biochem.* **1991**, *198*, 228−237.

(5) (a) Chang, T. C.; Kuo, C.-T.; Chiang, C. C.; Cheng, J.-Y.; Yan, C.-S.; Peck, K. *Phys. Chem. Chem. Phys.* **1999**, *1*, 3783−3787. (b) Yang, Y.-P.; Kuo, C.-T.; Yan, C.-S.; Lin, K.-C.; Huang, W.-C.; Chang, T.-C. *Phys. Chem. Chem. Phys.* **2000**, *2*, 5271−5274.

(6) (a) López Arbeloa, T.; López Arbeloa, F.; López Arbeloa, I.; García-Moreno, I.; Costela, A.; Sastre, R.; Amat-Guerri, F. *Chem. Phys. Lett.* **1999**, *299*, 315−321. (b) Costela, A.; García-Moreno, I.; Gomez, C.; Sastre, R.; Amat-Guerri, F.; Liras, M.; López Arbeloa, F.; Bañuelos Prieto, J.; López Arbeloa, I. *J. Phys. Chem. A* **2002**, *106*, 7736−7742. (c) López Arbeloa, F.; Bañuelos Prieto, J.; Martínez Martínez, V.; Arbeloa López, T.; López Arbeloa, I. *ChemPhysChem* **2004**, *5*, 1762−1771.

(7) Kollmannsberger, M.; Rurack, K.; Resch-Genger, U.; Daub, J. *J. Phys. Chem. A* **1998**, *102*, 10211−10220.

(8) Bañuelos Prieto, J.; López Arbeloa, F.; Martínez Martínez, V.; Arbeloa López, T.; Amat-Guerri, F.; Liras, M.; López Arbeloa, I. *Chem. Phys. Lett.* **2004**, *385*, 29−35.

(9) Wagner, R. W.; Lindsey, J. S. *Pure Appl. Chem.* **1996**, *68*, 1373−1380.

(10) Olmsted, J. *J. Phys. Chem.* **1979**, *83*, 2581−2584.

(11) (a) O'Connor, D. V.; Phillips, D. *Time-correlated Single Photon Counting*; Academic Press: New York, 1984. (b) Boens N. In *Luminescence*

Techniques in Chemical and Biochemical Analysis; Baeyens, W. R. G., De Keukeleire, D., Korkidis, K., Eds.; Marcel Dekker: New York, 1991; pp 21−45.

(12) Maus, M.; Rousseau, E.; Cotlet, M.; Schweitzer, G.; Hofkens, J.; Van der Auweraer, M.; De Schryver, F. C.; Krueger, A. *Rev. Sci. Instrum.* **2001**, *72*, 36−40.

(13) Crovetto, L.; Orte, A.; Talavera, E. M.; Alvarez-Pez, J. M.; Cotlet, M.; Thielemans, J.; De Schryver, F. C.; Boens, N. *J. Phys. Chem. B* **2004**, *108*, 6082−6092.

(14) Van den Zegel, M.; Boens, N.; Daems, D.; De Schryver, F. C. *Chem. Phys.* **1986**, *101*, 311−335.

(15) Kowalczyk, A.; Boens, N.; Van den Bergh, V.; De Schryver, F. C. *J. Phys. Chem.* **1994**, *98*, 8585−8590.

(16) Cielen, E.; Tahri, A.; Ver Heyen, A.; Hoornaert, G. J.; De Schryver, F. C.; Boens, N. *J. Chem. Soc., Perkin Trans. 2* **1998**, 1573−1580.

(17) (a) Pevenage, D.; Corens, D.; Van der Auweraer, M.; De Schryver, F. C. *Bull. Chem. Soc. Belg.* **1997**, *106*, 56. (b) Noukakis, D.; Van der Auweraer, M.; Toppet, S.; De Schryver, F. C. *J. Phys. Chem.* **1995**, *99*, 11860.

(18) Verbeek, G.; Depaemelaere, S.; Van der Auweraer, M.; De Schryver, F. C.; Vaes, A.; Terrell, D.; De Meutter, S. *Chem. Phys.* **1993**, *176*, 195.

(19) (a) Lippert, E. *Z. Naturforsch., A: Phys. Sci.* **1955**, *10*, 541. (b) Mataga, N.; Kaifu, Y.; Koizumi, M. *Bull. Chem. Soc. Jpn.* **1955**, *28*, 690.

(20) (a) Shen, Z.; Röhr, H.; Rurack, K.; Uno, H.; Spieles, M.; Schulz, B.; Reck, G.; Ono, N. *Chem.—Eur. J.* **2004**, *10*, 4853. (b) Picou, C. L.; Stevens, E. D.; Shah, M.; Boyer, J. H. *Acta Crystallogr.* **1990**, *C46*, 1148.

(21) Vranken, N.; Jordens, S.; De Belder, G.; Lor, M.; Rousseau, E.; Schweitzer, G.; Toppet, S.; Van der Auweraer, M.; De Schryver F. C. *J. Phys. Chem. A* **2001**, *105*, 10196.

(22) (a) Grabowski, Z. R.; Rotkiewicz, K.; Rettig, W. *Chem. Rev.* **2003**, *103*, 3899. (b) Jurczok, M.; Plaza, P.; Rettig, W.; Martin, M. M. *Chem. Phys.* **2000**, *256*, 137. (c) Mac, M.; Kwiatkowski, P.; Pischel, U. *Chem. Phys. Lett.* **2002**, *357*, 440. (d) Onkelinx, A.; De Schryver, F. C.; Viaene, L.; Van der Auweraer, M.; Iwai, K.; Yamamoto, M.; Ichikawa, M.; Masuhara, H.; Maus, M.; Rettig, W. *J. Am. Chem. Soc.* **1996**, *118*, 2892. (e) Herbich, J.; Kapturkiewicz, A. *Chem. Phys.* **1991**, *158*, 143.

(23) (a) Van Haver, P.; Helsen, N.; Depaemelaere, S.; Van der Auweraer, M.; De Schryver, F. C. *J. Am. Chem. Soc.* **1991**, *113*, 6849. (b) Verhoeven, J. W.; Scherer, T.; Wegewijs, B.; Hermant, R. M.; Jortner, J.; Bixon, M.; De Paemelaere, S.; De Schryver, F. C. *Recl. Trav. Chim. Pays-Bas* **1995**, *114*, 443. (c) Onkelinx, A.; De Schryver, F. C.; Schweitzer, G.; Miyasaka, H.; Van der Auweraer, M.; Asahi, T.; Masuhara, H.; Fukumura, H.; Yashima, A.; Iwai, K. *J. Phys. Chem. A* **1997**, *101*, 5054. (d) Tominaga, K.; Walker, G. C.; Kang, T. J.; Barbara, P. F.; Fonseca, T. *J. Phys. Chem.* **1991**, *95*, 10485. (e) Herbich, J.; Kapturkiewicz, A. *Chem. Phys.* **1991**, *158*, 143.

(24) (a) Boens, N.; Andriessen, R.; Ameloot, M.; Van Dommelen, L.; De Schryver, F. C. *J. Phys. Chem.* **1992**, *96*, 6331. (b) Boens, N.; Van Dommelen, L.; Ameloot, M. *Biophys. Chem.* **1993**, *48*, 301.

(25) (a) Boens, N.; Ameloot, M.; Hermans, B.; De Schryver, F. C.; Andriessen, R. *J. Phys. Chem.* **1993**, *97*, 799. (b) Van Dommelen, L.; Boens, N.; Ameloot, M.; De Schryver, F. C.; Kowalczyk, A. *J. Phys. Chem.* **1993**, *97*, 11738.

(26) Callan, J. F.; de Silva, A. P.; Ferguson, J.; Huxley, A. J. M.; O'Brien, A. M. *Tetrahedron* **2004**, *60*, 11125−11131.

(27) Werner, T.; Huber, C.; Heinl, S.; Kollmannsberger, M.; Daub, J.; Wolfbeis, O. S. *Fresenius J. Anal. Chem.* **1997**, *359*, 150−154.